Phys. Status Solidi A **212,** No. 8, 1695–1703 (2015) / **DOI** 10.1002/pssa.201532153

physica status solidi a
www.pss-a.com
applications and materials science

On the nature of defects produced by motion of dislocations in silicon

M. A. Khorosheva*,[1], V. V. Kveder,[1], and M. Seibt[2]**

[1] Institute of Solid State Physics, Russian Academy of Sciences, 2 Academician Ossipyan Str., 142432 Chernogolovka, Russia
[2] Georg-August-Universität Göttingen, IV. Physikalisches Institut, Friedrich-Hund-Platz 1, 37077 Göttingen, Germany

Received 10 March 2015, revised 30 April 2015, accepted 19 May 2015
Published online 12 June 2015

Keywords defect engineering, dislocations, DLTS, gold, point defects, silicon

* Corresponding author: e-mail khor@issp.ac.ru, Phone: 8(496)52 219 82, +7 (496) 52 223 44, Fax: +7(496) 522 8160
** e-mail kveder@issp.ac.ru

Point defects generated during motion of dislocations in silicon have been investigated using their reaction with gold atoms during gold in-diffusion. Deep Level Transient Spectroscopy (DLTS) measurements in n- and p-type samples have revealed that in regions with dislocation densities of 10^4–$10^6\,cm^{-2}$, the concentration of gold atoms is by 1.5–2 orders of magnitude higher than in the dislocation-free regions of the same samples. The increase in the gold atom concentration in the regions containing dislocations is explained by the presence of some vacancy complexes generated by dislocations moving in their slip planes. Just after dislocation motion, most of these complexes are not detectable by DLTS. They become observable in DLTS due to their reaction with gold atoms.

© 2015 WILEY-VCH Verlag GmbH & Co. KGaA, Weinheim

1 Introduction An important part of modern semiconductor technologies is "defect engineering," which allows controlled modification of electronic properties of semiconductors in desirable direction using the knowledge about interactions and reactions of various defects and impurities. At present, multicrystalline silicon is widely used for solar cell production. As it contains quite a high density of dislocations, the interaction of dislocations with impurities and point defects and their influence on electronic properties and electron-hole recombination in Si attracts considerable attention of researchers all over the world. Most of such investigations are focused on interaction of impurities with dislocations and on electronic properties of real dislocations with impurities and defects in their cores (e.g., see Refs. [1–7]).

At the same time, it was found experimentally in several publications that dislocations can generate some defects in dislocations slip planes during motion. Such a phenomenon was experimentally observed by using chemical etching in [8, 9]. EBIC experiments [9–13] also show that after plastic deformation of Si at 600–620 °C to a small dislocation density ($N_D \sim 10^5\,cm^{-2}$) not only dislocations, but also "dislocation trails" left behind moving dislocations, show EBIC contrast. Obviously, the nature and properties of those defects, as well, as the mechanism of their generation can be also interesting for defect engineering in solar cell technology. However, existing data about properties, nature, concentration and generation for such defects are still quite scarce, and contradicting.

To understand possible reasons for existing contradictions and bad reproducibility in electronic properties of "dislocation trail" defects, we hypothesized that the defects generated by moving dislocations are originally electrically inactive. We suppose that these defects can become electrically active due to their reactions with some transient metal impurities. As occasional contamination of samples at a temperature of 600 °C or higher to the level of impurity concentrations of the order of 10^{12}–$10^{13}\,cm^{-3}$ is nearly unavoidable, this hypothesis can explain bad reproducibility of results and some contradictions.

In this work, we made an attempt to check this hypothesis. The deep level transient spectroscopy (DLTS) was used to investigate n- and p-type silicon samples plastically deformed in conditions when the generation of "dislocation trail defects" can be expected as well as their significant contribution to electronic properties of the samples. To detect electrically inactive complexes of point defects occurring in the course of dislocation motion, we used a gold diffusion (see Refs. [15–17]).

2 Experimental Samples $32 \times 4 \times 1.3\,mm^3$ in size with their faces orientations being (1–10), (–1–12), and (111), were cut from silicon single crystals grown by

© 2015 WILEY-VCH Verlag GmbH & Co. KGaA, Weinheim

floating zone melting (Fz-Si). The n-type samples (with $n_{dop} = 10^{14}\,cm^{-3}$ phosphorous concentration) were used for DLTS studies of deep electronic states in the upper half of the energy band gap, and similar p-type samples (with $n_{dop} = 10^{14}\,cm^{-3}$ boron concentration) were used to study the levels in the lower half of the band-gap.

The "working surface" for introducing dislocations was the wide (111) face of the sample. To introduce the dislocation, we used a plastic deformation by four-point bending. Our idea was to have relatively small dislocation densities (10^4–$10^6\,cm^{-2}$) combined with a large dislocation glide distance S (from 400 to 1000 μm) implying the production of a large number of "dislocation trail defects." To reach this goal, we used a procedure to some extend similar to one used in by Refs. [9–12].

Following mechanical and chemical polishing, 2 mm long scratches were made on the working surface (Fig. 1) as dislocation sources. Subsequently, samples were deformed by four-point bending at 600 °C at a stress of about 20–30 MPa. At this stress dislocation, half loops with a radius of about 20–60 μm were generated from a scratches. Then we removed a scratch and its defected area by chemical etching to prevent further generation of dislocations. After that we again applied a stress of 20–30 MPa at 600 °C for 6–10 h by four-point bending. In this conditions, the dislocation generated during first stage were moving with a velocity of about 1–2 μm/min. As a result, we produced large dislocation half loops with a diameter from 0.8 to 2.0 mm. The dislocation density N_D for different samples varied from 10^4 to $10^6\,cm^{-2}$ as was measured by etch pit counting. Dislocation half loops consisting of 60° and screw

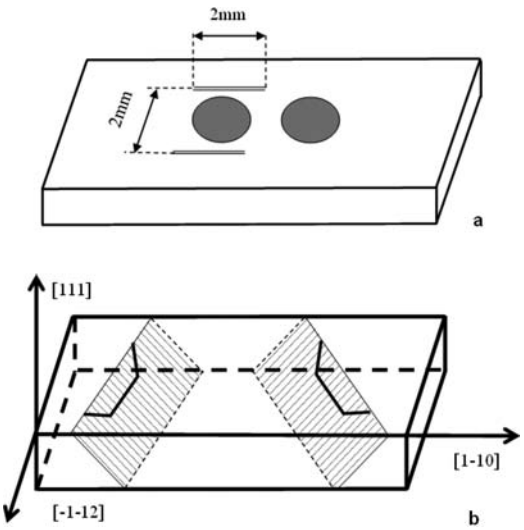

Figure 1 Schematic presentation of the sample geometry. (a) Position of 2 mm long scratches relative to circular Schottky contacts for DLTS measurements in areas with dislocations (left) and without dislocations (right). (b) Crystallographic directions glide planes and dislocation half-loop geometry.

segments were generated in two glide systems during such deformation as it is shown in Fig. 1b (see Ref. [18]).

After deformation, we removed a layer with a thickness of about 10 μm from the working surface by mechanical and chemical polishing.

During plastic deformation, the samples could be accidentally contaminated with some fast diffusing transition metal impurities. To reduce their concentration, we sometimes used the aluminum guttering (AlG) after plastic deformation. To this end, an aluminum layer was deposited on the working surface by thermal evaporation in vacuum and then the sample was placed into a quartz tube, held in a furnace in an argon flow at 800 °C for 2 h, and cooled down to 400 °C during 2 h. Subsequently, a 15 μm thick layer was removed from the working surface by mechanical polishing with diamond paste and chemically polished in $HF:7HNO_3$.

We should note that AlG procedure not only reduces the concentration of metal impurities in a sample, but also reduces the concentration of those defects that are thermally unstable at 800 °C. Some thermally unstable defects can also be destroyed during gold in-diffusion at 700 °C. We do not discuss those defects in this paper because they seem not to be so important for solar cell technology.

Gold in-diffusion was carried out at 700 °C for 3 h from the gold layer deposited in vacuum on the working surface. After diffusion, a 15 μm layer was removed from the surface by mechanical and chemical polishing.

To measure the DLTS spectra, two circular Schottky contacts 1.2 mm in diameter were deposited on the working surface by evaporation in vacuum of aluminum for p-type samples and gold for n-type samples, respectively. One of the Schottky contacts was formed in a sample region containing dislocations, while the other one in the region of the same sample without dislocations (Fig. 1a) serving as a reference. The dislocation density is, of course, quite non-uniform between scratches (Fig. 1a). So, when we speak about dislocation density N_D, we mean the average density of dislocations under the Schottky contact.

Immediately before the deposition of the Schottky contacts, the sample was chemically polished in $HF:7HNO_3$ for 10 s, then, it was held in $HF:10H_2O$ for 20 s to remove the oxide layer. In case of p-Si, samples were held under a tungsten lamp (40 W) at a distance of 15–20 mm for 10 min just before the deposition of Al contacts in order to form a fresh thin oxide layer. Ohmic contacts were formed on the back side of the sample by rubbing a Ga-Al alloy.

The dependences of DLTS spectra on a depth d under the sample surface were measured using layer-by-layer mechanical polishing with diamond paste followed by chemical polishing whereupon each time new Schottky contacts were deposited and DLTS spectra measured.

The DLTS spectra were measured at bias voltage $U_b = 5$ V. It corresponds to the thickness of depletion layer of about 7 μm under the Schottky contact. As DLTS signal is produced by recharging of deep level defects in this layer, the defect concentrations calculated from DLTS correspond to average value in a 7 μm layer under the surface. To

© 2015 WILEY-VCH Verlag GmbH & Co. KGaA, Weinheim

measure the electron or hole capture kinetics, we varied the refilling pulse duration t_p from 0.003 to 1 ms. To calculate activation energy for electron emission, we varied the emission transient time t_e from 500 to 12 ms, which correspond to a thermal emission rate $e_n(e_p) = 0.425/t_e$ from 0.85 to 35.6 s^{-1}.

3 Experimental results

3.1 DLTS before Au diffusion Figure 2a and b shows DLTS spectra measured in the regions containing dislocations of typical p- and n-type Si samples. Spectra (1) in both figures were measured just after plastic deformation. They consist of several overlapping broadened DLTS lines similar to those observed earlier in plastically deformed Si (e.g., see Refs. [14, 19–22]). However, the relative amplitude of those broad lines is different in different samples.

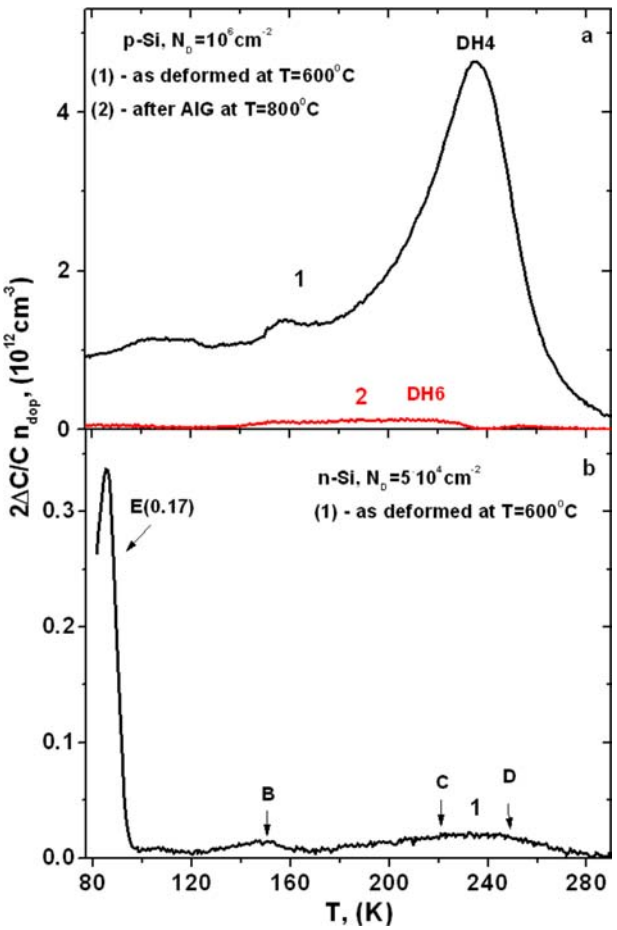

Figure 2 (a) Curve (1) is DLTS spectrum in a region with dislocation density of $N_D = 10^6\,cm^{-2}$ of as-deformed p-type sample, curve (2) is DLTS spectrum of the same region of the same sample after AlG. (b) DLTS spectrum in a region with dislocation density of $N_D = 5 \times 10^4\,cm^{-2}$ of as-deformed n-type sample. The labels B, C, D show positions of dislocation related lines according to classification of Ref. [19]. (DLTS was measured at $e_n(e_p) = 2.88\,s^{-1}$, $t_p = 0.1$ ms.)

As it was reported earlier, most of the defects corresponding to these broadened DLTS lines are thermally unstable and can be eliminated by thermal annealing at $T > 800\,°C$, while some of them (as line C) are very stable against annealing. Note that according to Refs. [7, 20, 22], the C-line corresponds to some impurities at dislocations. It means that the AlG should strongly decrease concentration of those defects in our samples. Curve (2) in Fig. 2a shows the DLTS spectrum measured after AlG in the same region of the same sample as spectrum (1) in Fig. 2a. One can see that, indeed, AlG does lead to a significant decrease in the concentration of all deep defects down to $10^{11}\,cm^{-3}$. The dislocation-free region of the same sample after AlG shows no DLTS signal higher than noise. The same was observed also for n-type samples.

Amplitudes of all DLTS lines in our as-deformed samples do not exceed values that can be expected for defects located at dislocations taking into account limitation coming from Coulomb interaction (e.g., see Refs. [19, 20]). We cannot exclude that some electrically active "dislocation trail defects" also give contribution to observed DLTS spectra, but in any case their concentration does not exceed $4 \times 10^{12}\,cm^{-3}$ for typical sample with $N_D = 10^6\,cm^{-2}$. It means that average concentration of electrically active "trail defects" per unit area of slip planes swept by moving dislocations is less than $4 \times 10^7\,cm^{-2}$. After AlG, the concentration of those defects becomes less than $10^6\,cm^{-2}$. Such a small concentration cannot strongly influence the solar cell efficiency.

However, as it was already mentioned in Introduction, we cannot exclude that a total concentration of the "trail defects" is much higher than $4 \times 10^7\,cm^{-2}$, but most of them are electrically inactive. To detect these defects, we used a diffusion of gold atoms. This method was developed by Refs. [15, 16]. It is based on the analysis of concentration profiles of electrically active substitutional gold Au_s (or platinum) atoms after their in-diffusion from the sample surface.

3.2 DLTS after Au diffusion Figure 3 presents the DLTS spectra of the p-type samples with different dislocation densities measured after gold in-diffusion at 700 °C.

In the spectra presented in Fig. 3a, five lines A1–A5 can be distinguished. The corresponding Arrhenius dependences of DLTS thermal emission rate on the line temperature positions for those DLTS lines are shown in Fig. 4.

As one can see in Fig. 3, the dominating line is A2. It corresponds to the well-known donor level $E_{Aud} = E_v + 0.33$ eV of substitutional gold atoms [Au_s] in silicon (e.g., see Ref. [23]).

The parameters of peak A5 coincide with those of the DLTS "Au + G4" center (see Ref. [23]) and corresponds to the acceptor level $E_{Aua} = E_C - 0.52$ eV of gold atoms Au_s. The small amplitude of peak A5 compared to that of peak A2 is fairly natural and is due to the fact that the E_{Aua} level is in the upper half of the energy band gap, and hence, closer to

© 2015 WILEY-VCH Verlag GmbH & Co. KGaA, Weinheim

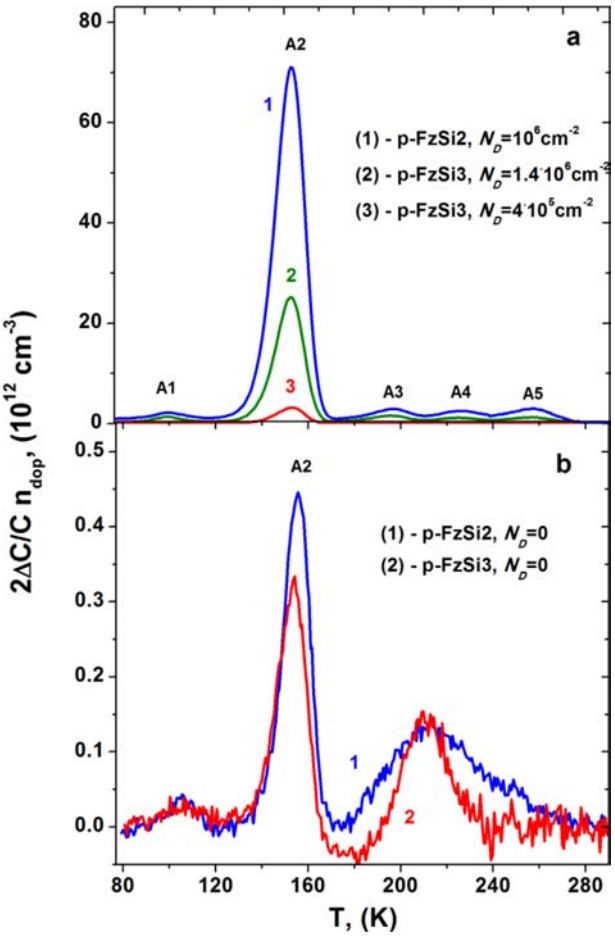

Figure 3 DLTS spectra of the p-type samples p-FzSi2 and p-FzSi3 after gold diffusion at 700 °C for 3 h. (a) Spectra measured in the regions with dislocations. A dominant signal at about $T = 154$ K corresponds to gold donor level. (b) Spectra measured in the dislocation-free regions of the same samples. Note that defect concentrations in dislocation-free regions (see (b)) are of about two orders of magnitude smaller compared to (a). (DLTS was measured at $e_p = 2.88\ s^{-1}$, $t_p = 0.1$ ms.)

the conduction band than to the valence band. In this case, the probability of thermal excitation of electrons into the conduction band exceeds the probability of excitation of holes into the valence band, which reduces significantly the effective amplitude of the DLTS peak. That is why the DLTS measurements in p-type samples are sufficiently correct only for the electronic states in the lower half of the band gap. In order to investigate the electronic states in the upper half of the band gap, measurements should be made in n-type samples.

The parameters of peak A3 are close to those of FeAu complex [24].

Peak A4 corresponds to some near-surface states (less than 2 μm from the surface) and, for this reason, is of no interest for us. Note that its parameters are close to the previously observed G3 line [23], which is likely to be connected with a hydrogen-containing complex.

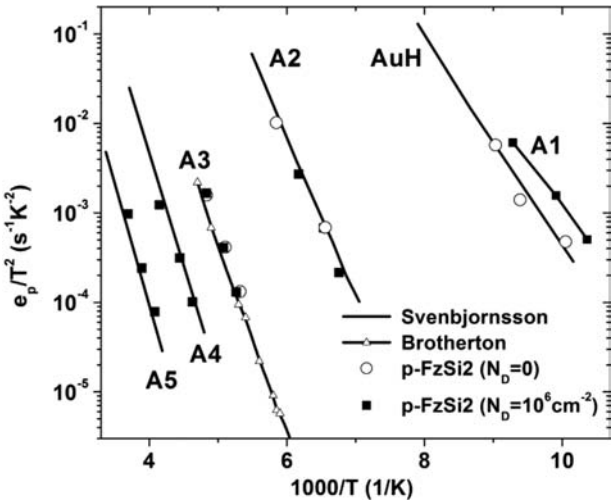

Figure 4 Arrhenius plots of thermal emission rate for peaks A1–A5 observed in DLTS spectra of p-type samples after gold diffusion. Curves with circles were obtained for the dislocation-free region, curves with squares for the region with a dislocation density of $10^6\ cm^{-2}$. Solid curves represent literature data of Sveinbjörnsson and Engström [23] and Brotherton et al. [24].

The position of peak A1 is formally close to that of the peak corresponding to the donor level of the Au–H complex previously observed by Ref. [23]. Yet, as seen in Fig. 4, the measured Arrhenius dependence for peak A1 is appreciably different from the data available in literature [23] for Au–H. Thus, the nature of this line remains unclear. Note, that parameters of DLTS peak at $T = 105$ K in dislocation free region of the same sample (Fig. 3b) coincide with those for Au–H complex and are different from A1.

The most interesting result of this Section is very strong dependence of concentration of substitutional gold atoms [Au_s] on dislocation density (Fig. 3). Note that [Au_s] is not proportional to dislocation density N_D. For example, [Au_s] in the sample with $N_D = 10^6\ cm^{-2}$ [see curve (1) in Fig. 3a] is significantly higher than the gold concentration [Au_s] in the sample with $N_D = 1.4 \times 10^6\ cm^{-2}$ [see curve (2) in Fig. 3a].

As it will be shown in Sections 4 and 5, this result agree well with our hypothesis that the gold concentration is connected to the concentration of electrically inactive "trail defects" generated by moving dislocations. Obviously, the concentration of those defects is rather proportional to the product of N_D and dislocation path S, than just to N_D.

The points shown in Fig. 5 indicate the gold atom concentrations [Au_s], estimated from the amplitude of DLTS peak A2 (gold donor), as functions of the depth d into the sample from the initial surface layer of gold used for in-diffusion. Filled squares show the data for the p-type sample obtained in the region with dislocation density $N_D = 1.6 \times 10^6\ cm^2$, while open circles show the data for [Au_s] in dislocation-free region of the same sample.

© 2015 WILEY-VCH Verlag GmbH & Co. KGaA, Weinheim

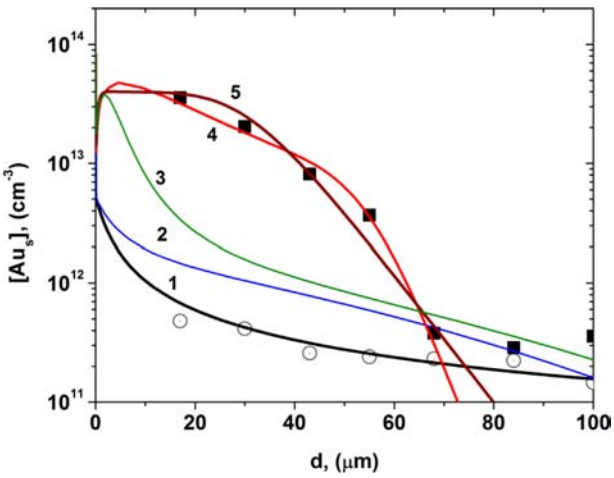

Figure 5 Experimental depth profiles of gold concentration [Au_s] obtained from amplitudes of A2 DLTS line (gold donor) in the dislocation-free region (open circles) and a region with a dislocation density of $N_D = 1.6 \times 10^6\,cm^{-2}$ (solid squares) after 3 h gold diffusion at 700 °C. Solid curves represent results of computer simulations for various parameters. Curve (1) corresponds to $N_D = 0$ and $[V]_{init} = [V]_{eq}$, curve (2) to $N_D = 1.6 \times 10^6\,cm^{-2}$, and $[V]_{init} = [V]_{eq}$. Curves (3), (4), (5) correspond to $N_D = 1.6 \times 10^6\,cm^{-2}$ and $[V]_{init} = 4 \times 10^{13}\,cm^{-3}$ (see text for details). Curve (3) is calculated assuming $D_V = 9.7 \times 10^{-9}\,cm^2\,s^{-1}$ and $r_{Au-V} = 1$ nm, curve (4) $D_V = 3 \times 10^{-10}\,cm^2\,s^{-1}$ and $r_{Au-V} = 0.15$ nm, curve (5) $D_V = 2 \times 10^{-12}\,cm^2\,s^{-1}$, and $r_{Au-V} = 0.01$ nm.

4 Computer simulation of gold in-diffusion To be able to compare our experimental data for [Au_s] gold profiles (Fig. 5) with what one can expect theoretically for different parameters of gold in-diffusion, we have performed computer simulations. For computer simulation, we used a standard set of 1D diffusion equations, similar to what was used by Refs. [15, 16, 25]. They describe the time evolution of concentration profiles for gold atoms in substitution positions Au_s, gold atoms in interstitial positions Au_i, Si-interstitial atoms I, and Si-vacancies V.

Both the kick-out reaction $Au_i \Leftrightarrow Au_s + I$ (see Ref. [26]) and Frank–Turnbull reaction $Au_i + V \Leftrightarrow Au_s$ [27] are taken into account. The standard set of equations also includes the reactions of vacancies and Si-interstitial atoms: $I + V \Leftrightarrow 0$.

To take into account also an influence of dislocations on diffusion, we included three additional reaction terms G_{I-D}, G_{V-D}, and G_{Au-D} into the set of equations earlier used by Refs. [15, 16, 25]. They describe diffusion-limited reactions of Si-interstitials (I), Si-vacancies (V), and interstitial gold atoms (Au_i) with dislocations. To estimate terms G_{I-D} and G_{V-D}, we supposed that the dislocation core serves as an ideal sink for I and V [28], so that it can be considered as a "black" cylinder with some radius R_{min}, where the concentrations of I and V are equal to the equilibrium values: $[I]_{R_{min}} = [I]_{eq}$, $[V]_{R_{min}} = [V]_{eq}$. We assumed that R_{min} is of the order of the lattice parameter L of Si crystal. So, for G_{I-D} we have

$$G_{I-D} = 2\pi N_D D_I \cdot \Big([I] - [I]_{eq}\Big) \Big/ \left(1 + \ln\frac{R_{max}}{L}\right), \quad (1)$$

where D_I is the diffusion coefficient of self-interstitial, and R_{max} is half of the distance between dislocations ($R_{max} \approx 0.5/N_D^{1/2}$). We supposed that the diffusion jump length is of about lattice parameter L, so that the diffusion jump frequency is equal to (D_I/L^2). The formula for G_{V-D} is similar to one for G_{I-D}.

The term G_{Au-D} corresponding to incorporation of Au_i atoms to dislocation cores is similar to Eq. (1), but it assumes that the number of places N_{core} in a dislocation core for Au atoms is limited. Assuming that an energy gain due to capture of Au_i atom into dislocation core is ΔH_{Aui}, and that $N_{core} \approx 1/L$, we have

$$G_{Au-D} \approx \frac{2\pi N_D D_{Au}}{1 + \ln\frac{R_{max}}{L} \cdot A} \times \left[[Au_i] \cdot A - [Au_D] \cdot L C_L \cdot \exp\left(-\frac{\Delta H_{Aui}}{kT}\right)\right]. \quad (2)$$

where $C_L \approx 5 \times 10^{22}\,cm^{-3}$ is the number of Si lattice sites per unit of volume and [Au_D] is the concentration of Au atoms captured at dislocation core per unit length implying [Au_D] $\cdot N_D$ to be the average concentration of captured Au atoms per unit volume. The coefficient A is $A = 1 - L[Au_D]$.

We assume $\Delta H_{Aui} = \Delta H_{Aus} + 0.8$ eV, where 0.8 eV is the energy difference between Au_i and Au_s atoms far from dislocation and ΔH_{Aus} is the energy difference between Au atom in dislocation core and Au_s atom far from dislocation. Estimations of ΔH_{Aus} using data obtained by neutron activation analysis in [29] give the value between 2.7 eV [29] and 1.5 eV [30]. We used the value $\Delta H_{Aus} = 1.5$ eV. However, the value of ΔH_{Aus} is not very critical for our calculation of Au_s profile. For $\Delta H_{Aus} = 2.7$ eV, the results for [Au_s] are similar.

The equilibrium concentrations and diffusion coefficients of vacancies and Si interstitials were recently specified in Ref. [25] using analysis of out-diffusion and in-diffusion profiles of Pt in a temperature range from 730 to 950 °C. According to Ref. [25], they can be calculated using the following expressions:

$$D_V = 0.4\exp(-1.47\,\text{eV}/kT)\ \text{cm}^2\text{s}^{-1}, \quad (3)$$

$$[V]_{eq} = 7.5 \times 10^{22}\exp(-2.56\,\text{eV}/kT)\ \text{cm}^{-3}, \quad (4)$$

$$D_I = 1.48 \times 10^3\exp(-1.77\,\text{eV}/kT)\ \text{cm}^2\text{s}^{-1}, \quad (5)$$

© 2015 WILEY-VCH Verlag GmbH & Co. KGaA, Weinheim

$$[\mathrm{I}]_{\mathrm{eq}} = 10^{23}\exp(-3.18\,\mathrm{eV}/kT)\ \mathrm{cm}^{-3}. \quad (6)$$

The parameters for gold diffusion were taken from Refs. [29–31]:

$$[\mathrm{Au_s}]_{\mathrm{eq}} = 6.4\times10^{24}\exp(-1.9\,\mathrm{eV}/kT)\ \mathrm{cm}^{-3}, \quad (7)$$

$$[\mathrm{Au_i}]_{\mathrm{eq}} = 6.4\times10^{24}\exp(-2.7\,\mathrm{eV}/kT)\ \mathrm{cm}^{-3}, \quad (8)$$

$$D_{\mathrm{Aui}} = 5\times10^{-5}\exp(-0.4\,\mathrm{eV}/kT)\ \mathrm{cm}^2\mathrm{s}^{-1}. \quad (9)$$

The theoretical curves shown in Fig. 5 represent the concentration profiles of substitution gold atoms [Au_s] calculated using our computer simulations of Au in-diffusion under various conditions differing in dislocation density N_D and initial vacancy concentrations $[V]_{init}$.

5 Discussion of results

5.1 Trail defects The most important experimental result to be explained is the anomalous excess concentration of gold [Au_s] in the dislocation-containing parts of samples compared to the dislocation-free parts of the same samples.

Curves (1) and (2) in Fig. 5 were calculated for initial concentrations of vacancy complexes $[V]_{init}$ and interstitial Si atoms $[I]_{init}$ equal to their equilibrium values given by Eqs. (4) and (6).

Curve (1) is calculated for dislocation density $N_D = 0$ and it correlates very well with experimental [Au_s] profiles in dislocation-free regions.

Curve (2) is calculated for dislocation density $N_D = 1.6\times10^6\,\mathrm{cm}^{-2}$. It is slightly higher than curve (1) due to the fact that dislocations are sinks for Si interstitials. This effect has been previously observed experimentally and is well understood (for instance, see Refs. [31, 33]). During diffusion of gold atoms, the kick-out mechanism $\mathrm{Au_i} \Leftrightarrow \mathrm{Au_s} + \mathrm{I}$ leads to a supersaturation of Si interstitials $[\mathrm{I}] \gg [\mathrm{I}]_{\mathrm{eq}}$ resulting in the reduction of [Au_s]. As dislocations act as good sink for Si interstitials, they reduce their concentration [I] thus increasing [Au_s].

However, as seen from Fig. 5, the experimentally measured concentration [Au_s] in the sample with $N_D \approx 1.6\times10^6\,\mathrm{cm}^{-2}$ is much higher than curve (2). So, a model exclusively assuming dislocations acting as perfect sinks for self interstitials and vacancies does not appropriately describe experimental data. Even when we assumed a much higher density of dislocations than the real one, we could not obtain a good correlation of calculated profile with experimental data.

In the following, a scenario will be developed that consistently explains the anomalously high concentration of [Au_s] in our samples under the assumption that dislocation motion (at 600 °C) generates non-equilibrium vacancy-type defects in the dislocation slip planes. In this case, an essential contribution to the gold diffusion process is made by the reaction $\mathrm{Au_i} + \mathrm{V} \Leftrightarrow \mathrm{Au_s}$ and the Au_s concentration can become almost equal to the initial concentration of vacancy-defects $[V]_{init}$ before Au diffusion.

The curves (4) and (5) shown in Fig. 5 show [Au_s] profiles calculated for initial concentration of vacancy-defects $[V]_{init} = 4\times10^{13}\,\mathrm{cm}^{-3}$. One can see that both curves correlate very good with experimental data measured in a region with dislocations.

The curve (4) was calculated assuming $D_V = 3\times10^{-10}\,\mathrm{cm}^2\,\mathrm{s}^{-1}$ and $\{\mathrm{V}+\mathrm{Au_i}\}$ reaction radius $r_{\mathrm{Au-V}} = 0.15\,\mathrm{nm}$, while the curve (5) was calculated with $D_V = 2\times10^{-12}\,\mathrm{cm}^2\,\mathrm{s}^{-1}$ and $r_{\mathrm{Au-V}} = 0.01\,\mathrm{nm}$. If the diffusion coefficient D_V of vacancy defects is below $3\times10^{-10}\,\mathrm{cm}^2\,\mathrm{s}^{-1}$, the calculated data fit well to experimental one.

However, the [Au_s] profile calculated for the value $D_V = 9.7\times10^{-9}\,\mathrm{cm}^2\,\mathrm{s}^{-1}$ giving by Eq. (3) at 700 °C does not agree with the experimental data [see curve (3) in Fig. 5]. It means that the vacancy-type defects produced by moving dislocations are not just vacancies, but some vacancy complexes with effective diffusion coefficient much smaller than one giving by Eq. (3).

As these vacancy-type defects assumed to be generated in dislocation slip planes, their distribution should be strongly non-uniform. However, DLTS data obtained in p-type samples cannot prove it. Probably, the distribution of vacancy-defects becomes more uniform during AlG at 800 °C performed for p-type samples after plastic deformation.

For some n-type samples, the AlG was not performed before gold in-diffusion. Figure 6 shows the DLTS spectra measured in such a sample in the region containing dislocations after gold diffusion at 700 °C.

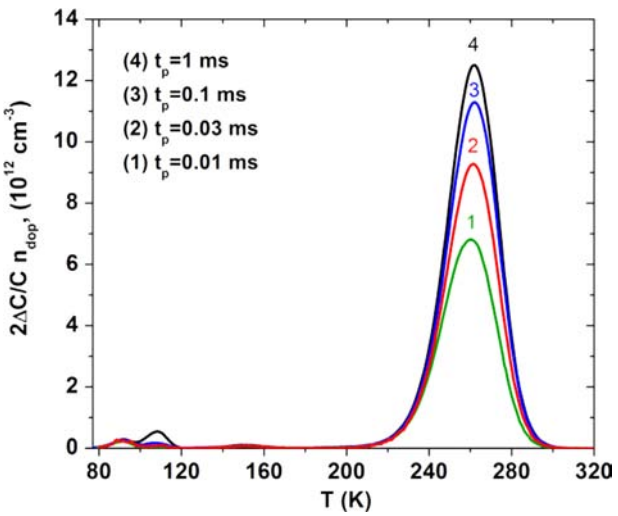

Figure 6 DLTS spectra of the n-type sample without AlG after gold diffusion at $T = 700$ °C for 3 h obtained in the dislocation region ($N_D = 5\times10^4\,\mathrm{cm}^{-2}$) for different filling pulse durations t_p. A logarithmic filling pulse kinetics as a fingerprint of barrier-limited capture is observed for the gold acceptor. (DLTS was measured at $e_n = 2.88\,\mathrm{s}^{-1}$.)

© 2015 WILEY-VCH Verlag GmbH & Co. KGaA, Weinheim

The dominating peak at 262 K with $E_{Aua} = E_c - 0.52$ eV corresponds to the acceptor level of Au_s [34]. One can see that the amplitude of this DLTS peak logarithmically depends on the filling pulse duration. The observed logarithmic dependence of the Au_s peak amplitude on t_p provides evidence a strongly non-uniform distribution of Au_s gold atoms giving rise to a charge-dependent Coulomb barrier around the gold "clouds" with a high local concentration of $[Au_s]_{Loc} > n_{dop}$ upon capture of electrons by Au_s. A consistent scenario is obtained supposing that the "clouds" are located in the vicinity of dislocation slip planes where the vacancy defects were produced by dislocation motion. The diffusion coefficient D of these defects at 700 °C is obviously small enough to preserve strongly non-uniform distribution of vacancy defects before their reaction with gold atoms.

The final point to be discussed in the remaining part of this section is related to the electrical activity of Au atoms collected in dislocation cores subsequently referred to as Au_D.

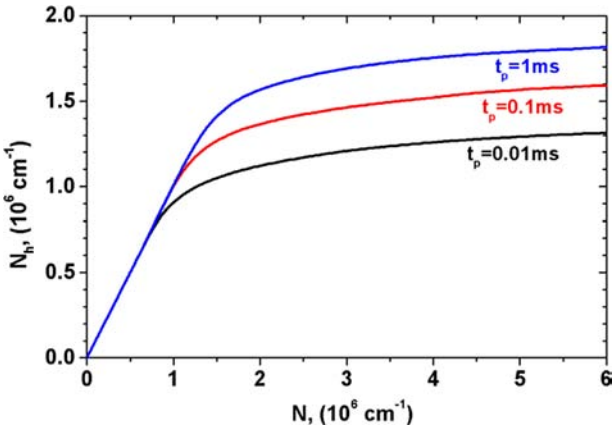

Figure 7 Line concentration of holes N_h captured by dislocation traps during time t_p as a function of dislocation trap concentration N as calculated for p-type Si using Eqs. (10) and (11) with parameters $E_{Aud} = E_V + 0.33$ eV, $\sigma = 8.6 \times 10^{-15}$ cm^2, exp$(\Delta S/k) = 2.4$, $n_{dop} = 10^{14}$ cm^{-3}, $T = 154$ K.

6 Gold at dislocations As we have already mentioned, it was shown by Ref. [29] using neutron activation experiments that the binding energy of gold atoms to dislocation ΔH_{Aus} is very large. It means, dislocations should capture a lot of gold. Our computer simulations have been made assuming a binding energy of Au atoms to the dislocation core of $\Delta H_{Aus} = 1.5$ eV (see Ref. [30]) and predict a gold concentration at dislocations of about $[Au_D] \approx 10^7$ cm^{-1} at the depth $d = 20$ μm below the surface. Hence, the total number of Au atoms captured by dislocations is of the order of $[Au_D] \cdot N_D \approx 1.6 \times 10^{13}$ cm^{-3}.

However, the amplitude of DLTS peak related to the gold atoms at dislocations must be much smaller than calculated value of $[Au_D] \cdot N_D$ because the DLTS is proportional not to the number of defects, but to the number of electrons (or holes) captured by defects. In case of dislocations, it is limited by the repulsive Coulomb potential of charged dislocations. This is shown in Fig. 7, which shows the calculated amplitude of a DLTS line equal to concentration of holes N_h captured at acceptor level of gold atoms during filling pulse t_p depending on concentration N of gold atoms in dislocation core ($N = [Au_D]$). The calculations were made for typical conditions of our DLTS measurements in p-type Si assuming that parameters of acceptor states are similar to those for Au_s and the energy level of Au_D atoms are not broadened due to interactions with the dislocation or interactions between Au_D centers. The following kinetic equation for hole capture to deep-level defects at dislocation was used for calculation (e.g., see Refs. [6, 20])

$$\frac{\partial N_h}{\partial t} = \sigma v n_{dop}(N - N_h)\exp\left(\frac{e\varphi}{kT}\right) - \sigma v N_h N_v \exp\left(-\frac{E_{Aud} - E_v + T\Delta S}{kT}\right). \quad (10)$$

Here σ is the cross-section of hole capture by Au_D, E_{Aud} is the donor level of gold atoms in the dislocation core, ΔS is the entropy change caused by hole capture, v is the thermal velocity of free holes, N_v is the effective density of states in the valence band, and n_{dop} is the concentration of free holes equal to the concentration of shallow acceptors ($n_{dop} = 10^{14}$cm^{-3}). The factor $e\varphi$ is a Coulomb potential at dislocations which slows down further capture of holes to dislocation line

$$e\varphi = \frac{e^2 N_h}{2\pi\varepsilon\varepsilon_0}\left\{\left[\ln\frac{{N_h}^{3/2}}{\sqrt{\pi n_{dop}}}\right] - 0.5\right\}, \quad (11)$$

where ε is the static dielectric constant (for Si: 11.9), $\varepsilon_0 = 8.854 \times 10^{-12}$ A s V^{-1}m^{-1} is the permittivity of free space.

As one can see, the DLTS amplitude only corresponds to the total defect concentration, i.e., $N_h \approx N$, if $N < 10^6$ cm^{-1} corresponding to weak binding of Au to dislocation core sites. At large N, the concentration of holes captured by such sites produces a DLTS signal with a sub-linear (logarithmic) dependence on the number of gold atoms at dislocation core sites. At $N = [Au_D] \approx 10^7$ cm^{-1} estimated from our simulations, the DLTS signal will correspond only to 16% of Au atoms captured on dislocations. For the situation in our experiments, it means that for the total number of Au atoms at dislocation core sites of about 1.6×10^{13} cm^{-3} the amplitude of DLTS signal will correspond to the value of about 2×10^{12} cm^{-3}. That is 10 times smaller than observed amplitude of DLTS signal from Au_s around dislocations slip-planes.

Therefore, for $N_D = 1.6 \times 10^6$ cm^{-2}, we can expect a DLTS peak related to Au_D with an amplitude of the order of 2×10^{12} cm^{-3} and with logarithmic dependence of its amplitude on t_p duration. Note, that the values of σ and E_{Aud}

© 2015 WILEY-VCH Verlag GmbH & Co. KGaA, Weinheim

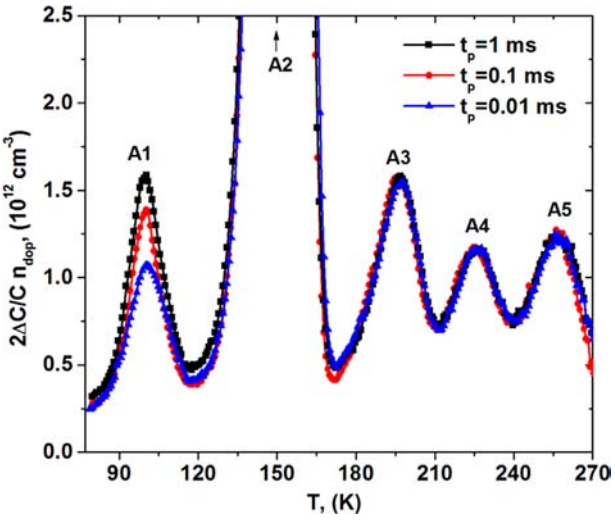

Figure 8 DLTS spectra as functions of filling pulse duration for the p-type Si sample with a dislocation density of $N_D = 1.6 \times 10^6$ cm^{-2} obtained after Au diffusion. Level A1 clearly shows barrier-limited capture kinetics. (DLTS was measured at $e_p = 2.88\,s^{-1}$.)

is for gold in dislocation core can be significantly different from those for Au_s in the bulk of Si as was shown, e.g., for copper by *ab initio* calculations (e.g., see Ref. [35]).

The scaled-up DLTS spectra of one of the p-type samples with dislocations after gold diffusion are shown in Fig. 8. One can see that the peak A1 can be a candidate for the DLTS signal of Au_D at dislocations. However, we are not convinced that peak A1 actually corresponds to the gold at dislocations. We cannot exclude the possibility that the DLTS peak related Au_D is so strongly broadened that it cannot be distinguished in DLTS spectra of our samples. More than that, at the moment we even cannot exclude the possibility that gold at dislocation is not electrically active at all. Obviously, the question about electronic properties of gold atoms captured in the dislocation core is still open and needs further investigation.

7 Conclusions In conclusion, samples with dislocation densities of 10^4–$10^6\,cm^{-2}$ deformed at $T = 600\,^\circ C$ and subsequent gold in-diffusion at $700\,^\circ C$ exhibit a large increase in the concentration of substitutional gold atoms, which can only be explained assuming that motion of dislocations in their glide planes gives rise to vacancy defects. The latter are vacancy complexes giving rise to an effective vacancy diffusion coefficient about four orders of magnitude below that of isolated vacancies. They strongly influence the gold diffusion process.

From kinetics measured by DLTS it has been deduced that the vacancy complexes have an inhomogeneous spatial distribution. From this it may be concluded that the so-called "dislocation traces" previously observed in [8–13] by selective chemical etching and by EBIC are related to such vacancy complexes. This has been proposed previously by Eyidi et al. [36] based on dislocation microstructure investigations on the temperature and stress regime of trail formation. Atomistic calculations have revealed dislocation dipole annihilation as a possible source of vacancy clusters [37, 38]. Our DLTS experiments did not exhibit any deep levels that might be associated with such complexes prior to gold in-diffusion which seems to be in conflict with the electrical activity of traces observed by EBIC and thus with the above interpretation. This apparent contradiction points to an important issue, i.e., the interaction of fast diffusing impurities with the vacancy complexes. In fact, our gold marker experiments provide evidence that metal impurities will strongly enhance the electrical activity of vacancy defects by reaction with interstitial metal impurities. Therefore, one cannot exclude that observation of "dislocation traces" by EBIC in as-deformed samples can be a result of their slight occasional contamination by transient metal impurities during plastic deformation.

Finally, we want to mention that our results might shed new light on a longstanding problem of multi-crystalline silicon materials for photovoltaic applications, i.e., existence of highly stressed regions which exhibit recombination activity [39] and can hardly be improved by gettering procedures [40]. In such highly stressed regions, dislocations are likely to move during processing possible leading to the formation of vacancy complexes by moving dislocations and their decoration by fast diffusing metal impurities. Such metal-vacancy complexes can be extremely stable [41, 42], i.e., they are rather inert against gettering processes. As dislocation movement is the key to vacancy complex formation rather than their mere existence new strategies of defect engineering need to be developed to handle this efficiency-limiting problem of silicon photovoltaics.

Acknowledgements This work was supported in part by research program "Physics of novel materials and structures" of Russian Academy of Sciences and by the President grant NSh-884.2014.2.

References

[1] V. Higgs and M. Kittler, Appl. Phys. Lett. **65**, 2804 (1994).
[2] B. Shen, T. Sekiguchi, and K. Sumino, Jpn. J. Appl. Phys. **35**, 3301 (1996).
[3] M. Kittler, W. Seifert, and V. Higgs, Phys. Status Solidi A **137**, 327 (1993).
[4] V. Kveder, T. Sekiguchi, and K. Sumino, Phys. Rev. B **51**, 16721 (1995).
[5] V. Kveder, M. Kittler, and W. Schröter, Phys. Rev. B **63**, 115208 (2001).
[6] W. Schröter and H. Cerva, Sol. Stat. Phenom. **85–86**, 67 (2002).
[7] V. Kveder, V. Orlov, M. Khorosheva, and M. Seibt, Solid State Phenom. **131–133**, 175 (2008).
[8] I. E. Bondarenko, V. G. Eremenko, B. Ya. Farber, V. I. Nikitenko, and E. B. Yakimov, Phys. Status Solidi A **68**, 53 (1981).
[9] V. Eremenko, E. Yakimov, and N. Abrosimov, Phys. Status Solidi C **4**, 3100 (2007).
[10] O. V. Feklisova and E. B. Yakimov, Phys. Status Solidi C **4**, 3105 (2007).

© 2015 WILEY-VCH Verlag GmbH & Co. KGaA, Weinheim

[11] O. V. Feklisova, E. B. Yakimov, N. Yarykin, and B. Pichaud, J. Phys.: Condens. Matter **16**, 201 (2004).
[12] O. V. Feklisova, B. Pichaud, and E. B. Yakimov, Phys. Status Solidi A **202**, 896 (2005).
[13] O. V. Feklisova, E. B. Yakimov, and N. Yarykin, Physica B **340-342**, 1005 (2003).
[14] M. Acciarri, S. Binetti, O. V. Feklisova, E. A. Steinman, and E. B. Yakimov, Solid State Phenom. **95-96**, 453 (2004).
[15] H. Zimmermann and H. Ryssel, Appl. Phys. A **55**, 121 (1992).
[16] M. Jacob, P. Pichler, H. Ryssel, and R. Falster, J. Appl. Phys. **82**, 182 (1997).
[17] M. A. Khorosheva, V. I. Orlov, N. V. Abrosimov, and V. V. Kveder, JETP **110**, 769 (2010).
[18] V. N. Erofeyev, V. I. Nikitenko, V. I. Polovinkina, and E. V. Suvorov, Crystallogr. Rep. **16**, 190 (1971).
[19] P. Omling, E. Weber, L. Montelius, H. Alexander, and J. Michel, Phys. Rev. B **32**, 6571 (1985).
[20] V. V. Kveder, Yu. A. Osipian, W. Schröter, and G. Zoth, Phys. Status Solidi A **72**, 701 (1982).
[21] L. C. Kimerling and J. R. Patel, Appl. Phys. Lett. **34**, 73 (1979).
[22] V. Kveder, M. Badylevich, E. Steinman, A. Izotov, M. Seibt, and W. Schröter, Appl. Phys. Lett. **84**, 2106 (2004).
[23] E. O. Sveinbjörnsson and Q. Engström, Phys. Rev. B **52**, 4884 (1995).
[24] S. D. Brotherton, P. Bradley, A. Gill, and E. R. Weber, J. Appl. Phys. **55**, 952 (1984).
[25] E. Badr, P. Pichler, and G. Schmidt, J. Appl. Phys. **116**, 133508 (2014).
[26] U. Gösele, W. Frank, and A. Seeger, Appl. Phys. **23**, 361 (1980).
[27] F. C. Frank and D. Turnbull, Phys. Rev. **104**, 617 (1956).
[28] T. L. Larsen, L. Jensen, A. Ludge, H. Riemann, and H. Lemke, J. Cryst. Growth **230**, 300 (2001).
[29] A. Rodriguez, H. Bracht, and I. Yonenaga, J. Appl. Phys. **95**, 7841 (2004).
[30] O. Voss, PhD thesis, Göttingen University, 2009; http://hdl.handle.net/11858/00-1735-0000-0006-B488-5
[31] N. A. Stolwijk, J. Holzel, W. Frank, E. R. Weber, and H. Mehrer, Appl. Phys. A **39**, 37 (1986).
[32] H. Bracht, N. A. Stolwijk, and H. Mehrer, Phys. Rev. B **52**, 16542 (1995).
[33] E. Yakimov, G. Mariani, and B. Pichaud, J. Appl. Phys. **78**, 1495 (1995).
[34] L. Rubaldo, P. Deixler, I. D. Hawkins, J. Terry, D. K. Maude, J.-C. Portal, J. H. Evans-Freeman, L. Dobaczewski, and A.R. Peaker, Mater. Sci. Eng. B **58**, 126 (1999).
[35] N. Fujita, R. Jones, S. Oberg, P. Briddon, and A. Blumenau, Solid State Phenom. **131–133**, 259 (2008).
[36] D. Eyidi, V. Eremenko, J. L. Demenet, and J. Rabier, Physica B **404**, 4634 (2009).
[37] J. Rabier and L. Pizzagalli, J. Phys. Conf. Ser. **281**, 012025 (2011).
[38] J. Rabier, Philos. Mag. **93**, 162 (2013).
[39] G. Sarau, S. Christiansen, M. Holla, and W. Seifert, Sol. Energy Mater. Sol. Cells **95**, 2264 (2011).
[40] M. Seibt and V. Kveder, Advanced Silicon Materials for Photovoltaic Applications (Wiley, New York, 2012), chap. 4, pp. 127.
[41] S. K. Estreicher, M. Sanati, and N. Gonzalez Szwacki, Phys. Rev. B **77**, 125214 (2008).
[42] D. J. Backlund and S. K. Estreicher, Phys. Rev. B **81**, 235213 (2010).

© 2015 WILEY-VCH Verlag GmbH & Co. KGaA, Weinheim